Soft Matter

Cite this: *Soft Matter*, 2011, **7**, 3524

www.rsc.org/softmatter

PAPER

Interfiber interactions alter the stiffness of gels formed by supramolecular self-assembled nanofibers†

Yavuz S. Dagdas, Aysegul Tombuloglu, Ayse B. Tekinay, Aykutlu Dana* and Mustafa O. Guler*

Received 2nd October 2010, Accepted 6th January 2011
DOI: 10.1039/c0sm01089h

Molecular self-assembly is a powerful technique for developing novel nanostructures by using non-covalent interactions such as hydrogen bonding, hydrophobic, electrostatic, metal–ligand, π–π and van der Waals interactions. These interactions are highly dynamic and are often delicate due to their relatively weak nature. However, a sufficient number of these weak interactions can yield a stable assembly. In this work, we studied the mechanical properties of self-assembled peptide amphiphile nanostructures in the nanometre and micrometre scale. Hydrogen bonding, hydrophobic and electrostatic interactions promote self-assembly of peptide amphiphile molecules into nanofibers. Bundles of nanofibers form a three-dimensional network resulting in gel formation. The effect of the nanofiber network on the mechanical properties of the gels was analyzed by AFM, rheology and CD. Concentration and temperature dependent measurements of gel stiffness suggest that the mechanical properties of the gels are determined by a number of factors including the interfiber interactions and mechanical properties of individual nanofibers. We point out that the divergence in gel stiffness may arise from the difference in strength of interfiber bonds based on an energetic model of elastic rod networks, along with continuum mechanical models of bundles of rods. This finding differs from the results observed with traditional polymeric materials. Understanding the mechanisms behind the viscoelastic properties of the gels formed by self-assembling molecules can lead to development of new materials with controlled stiffness. Tissue engineering applications can especially benefit from these materials, where the mechanical properties of the extracellular matrix are crucial for cell fate determination.

Introduction

Self-assembled nanostructures have extensively been used in various applications where nanoscale properties have important effects on function. These nanostructures are usually formed by small molecules through non-covalent interactions and the assembly mechanisms are sensitive to changes in the environment.[1–3] Peptide amphiphiles (PA) are self-assembling molecules that form nanofibers because of hydrogen bonds[4] and hydrophobic forces.[5] The peptide segment in the PA molecules directs β-sheet formation through hydrogen bonding and the alkyl groups results in micelle formation through hydrophobic collapse in an aqueous environment. The hydrogen bonded network of the peptide sequence is affected by electrostatic interactions and causes the formation of nanofiber-like cylindrical micelles instead of spherical micelles.[2,4,6–9] The network of PA nanofibers form a three-dimensional (3-D) structure resulting in gel formation in aqueous conditions.[3,4,10–13]

The gels formed by PA molecules are finding applications as scaffolds for tissue engineering due to their ability to mimic the native extracellular matrix (ECM).[8,13–16] The ECM supports the attachment, proliferation and migration of cells and provides structure to tissue. The mechanical surroundings of cells can result in alterations in cellular response through cytoskeletal structure, thus affecting the cell behavior and direct stem cell differentiation.[17–19] Therefore, it is essential to control the mechanical features of the scaffolds as well as their bioactivity for tissue engineering applications.

Mechanical features of PA gels can be tuned for various tissue engineering approaches depending on tissue type. The PA molecules form a dynamic assembly which is affected by pH change, electrolyte addition and electrostatic interactions. Thus, a better understanding of the gelation mechanisms of PA molecules will help us design appropriate substrates for tissue engineering studies. The self-assembled PA nanostructures differ from traditional polymeric materials in terms of 3-D interactions. The mechanical properties of the networks formed by polymeric nanostructures are usually directly related to material concentration.[20,21] An increase in the concentration results in the

UNAM-Institute of Materials Science and Nanotechnology, Bilkent University, Ankara, 06800, Turkey. E-mail: moguler@unam.bilkent.edu.tr; aykutlu@unam.bilkent.edu.tr; Fax: + 90 312 2664365; Tel: + 90 312 290 3552

† Electronic supplementary information (ESI) available: Additional experimental details. See DOI: 10.1039/c0sm01089h

extension of the nanostructures and the interaction between the nanostructures results in enhanced stiffness at the microscale. However, the microscale mechanical properties of PA based networks are not affected by interactions among the nanostructures in a similar fashion to polymeric systems due to their dynamic nature. Therefore, it is important to understand the relationship between nanometre and micrometre scale mechanical properties of self-assembled materials.

In this work, we studied the mechanical properties of gels formed through solvent encapsulation by self-assembled PA nanofibers. The effect of the mechanical properties of nanofibers on the gel stiffness was studied by AFM (atomic force microscopy), rheology and CD (circular dichroism). Our results suggest that interfiber interactions are an important factor contributing to the gel stiffness in addition to the mechanical properties of individual nanofibers.

Materials and methods

Materials

Fmoc protected amino acids, Fmoc–Asp–(OtBu)–Wang resin and HBTU were purchased from NovaBiochem and ABCR. The other chemicals were purchased from Fisher, Merck, Alfa Aesar or Sigma-Aldrich and used as received, without any purification.

Peptide design and synthesis

The PA molecule used in this study is composed of an alkyl group (lauric acid), a β-sheet forming (VVAG) peptide sequence followed by a glutamic acid residue, which is effective in increasing the solubility of the molecule, and a bioactive epitope (RGD), a peptide sequence that enhances cell adhesion (Fig. 1).[22]

PA molecules were synthesized by using solid phase fluorenylmethoxycarbonyl (Fmoc) peptide synthesis method. The synthesis was performed manually on a 0.25 mmol scale using a 50 ml peptide synthesis vessel on a wrist action shaker. PA molecules were synthesized by using a Fmoc–Asp–(OtBu)–Wang resin. After each reaction, the resin was washed three times with DMF (*N*,*N*-dimethylformamide), DCM (dichloromethane) and DMF. All the amino acids were activated by adding 2 molar equivalents of amino acid to 1.95 equivalents of *o*-benzotriazole-*N*,*N*,*N*′,*N*′-tetramethyl-uronium-hexafluoro-phosphate (HBTU) and dissolved in DMF. After complete dissolution of the amino acid and HBTU in DMF, 3 molar equivalents of *N*-ethyl-diisopropylamine (DIEA) was added to the solution. The solution was mixed thoroughly and left for 3 min before it was added to the resin. Each amino acid attachment was performed for 2.5 h. For each coupling reaction, the Fmoc groups were removed by shaking the resin in 20% piperidine in DMF for 20 min. The alkylation reaction was performed by coupling the peptide with lauric acid. Lauric acid coupling was performed in the same manner as for the amino acids. A ninhydrin test was performed after addition of each amino acid and after addition of the fatty acid. When the ninhydrin test yielded positive results, the coupling reaction was repeated; otherwise 10% acetic anhydride in DMF was added and the resin was shaken for 30 min. Peptide cleavage from the resin and deprotection of the amino acid side chains were performed with 95 : 2.5 : 2.5 trifluoroacetic acid (TFA) : triisopropylsilane (TIS) : water for 2.5 h at room temperature. After the cleavage reaction, PA molecules were collected in a clean round bottom flask and washed several times with DCM. The collected solution was rotary-evaporated. After evaporation, ice-cold diethyl ether was added to the peptide solution and was left at −20 °C overnight. The PA and diethyl ether mixture was collected in 50 ml falcon tubes and centrifuged at 8000 rpm for 25 min. The supernatant was decanted and the remaining peptide sample dissolved in deionized water at a resistance of 18.2 Ω and was freeze-dried. The identity and purity of the PA were assessed using an Agilent 6530–1200 Q-TOF LC-MS equipped with ESI-MS and a Zorbax Extend C18 column (Agilent 4.6 × 100 mm, 3.5 μm). A: 0.1% ammonium hydroxide in water and B: 0.1% ammonium hydroxide in acetonitrile gradients were used for analytical and preparative RP-HPLC. (Fig. S1 and S2, ESI†)

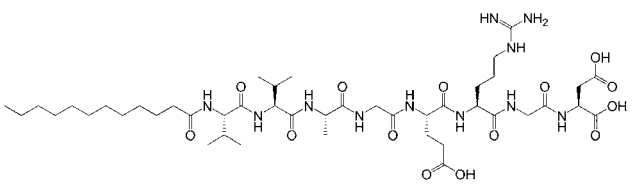

Fig. 1 Chemical structure of the investigated peptide amphiphile molecule.

Scanning electron microscopy (SEM)

The nanofiber networks formed by the PA molecules were observed using scanning electron microscopy (SEM). SEM samples of the PA with HCl gels and the PA with $CaCl_2$ gels were prepared at final PA and gelator concentrations of 8.3 mM and 41.7 mM respectively. The PA with HCl samples had a final pH of 2 and the PA with $CaCl_2$ gels were mixed at 1 : 5 molar ratios. The gels were then placed onto a metal mesh and dehydrated with increasing concentrations of ethanol up to 100%. The ethanol was then removed by critical point drying (Tousimis, Autosamdri-815B). The samples were then sputter-coated twice with 2.5 nm of Pt to ensure a complete coating. Visualization of the nanofiber networks were carried out with an FEI, Nova NanoSEM 430 scanning electron microscope at 18 kV with an average working distance of 5 mm.

Transmission electron microscopy (TEM)

PA solution mixed with $CaCl_2$ and PA solution mixed with HCl were prepared for TEM. 10 μl of 2 mM PA solution at pH 7 was mixed with 2 μl of 250 mM $CaCl_2$ solution and 10 μl of 2 mM PA solution at pH 7 was mixed with 2 μl of 250 mM HCl solution. The PA with $CaCl_2$ and the PA with HCl solutions were cast onto TEM grids and incubated for 3 min. Samples were stained with 2 wt% aqueous uranyl acetate solution then air dried overnight. TEM images were acquired with an FEI Tecnai G2 F30 TEM at 100 kV.

Atomic force microscopy (AFM) and force spectroscopy

AFM samples were prepared on 1 cm^2 silicon wafers (with low residual roughness (<1 nm μm^{-2})) using 25 μl of 0.5 mM PA

solutions. PA with $CaCl_2$ samples were prepared by mixing 100 μl of 0.5 mM PA solution at pH 7 with 3 μl of 50 mM $CaCl_2$ solution (1 : 3 molar ratio). PA with HCl samples were prepared by adjusting the final pH to 2. After addition of $CaCl_2$ and HCl to the pH 7 PA solution, eppendorf vials were vortexed thoroughly and sonicated for 5 min. 1 min after casting the solution onto a silicon wafer, excess water was removed with a tissue and the sample was air dried. Dynamic and contact mode imaging were used to image the topography of the resulting samples, using appropriate cantilevers (a cantilever stiffness of $k = 3$–40 N m^{-1}, resonance frequency of $f_0 = 70$–350 kHz was used for the dynamic mode and a cantilever stiffness of $k = 0.05 \pm 0.2$ N m^{-1} for the contact mode). Force–distance measurements were performed to estimate the elastic moduli of films at locations with thickness greater than ~50 nm.[23]

Circular dichroism (CD) (at room temperature)

CD spectra of the PA solutions were obtained using a J-815 Jasco spectrophotometer in the far UV region (190–300 nm) using quartz cuvettes with 1 mm path length. All of the samples that were used in the room temperature CD studies were prepared from the same batch and the pH was adjusted to 7 before use. The spectra were acquired for three formulations; PA at pH 7, PA mixed with $CaCl_2$ solution and PA mixed with HCl solution. The PA with HCl sample was prepared by adjusting the pH to 2 and the PA with $CaCl_2$ sample was prepared by adding $CaCl_2$ at 1 : 5 molar ratios compared to the PA to ensure complete neutralization of the charges at pH 7. A solution of 0.1 mM PA was prepared in deionized water and the pH was adjusted to 7. For the PA with $CaCl_2$ measurements, 5 μl of 100 mM $CaCl_2$ was added to 1 ml of PA solution. For the PA with HCl measurements, the pH of a 1 ml sample of the PA solution was adjusted to pH 2 with HCl solution. Averages of three scans of each sample were taken.

In order to study the effect of $CaCl_2$ on secondary structure formation, the CD spectra were monitored after adding EDTA to the PA with $CaCl_2$ sample. 2.6 ml of 7 mM $CaCl_2$ was added to 400 μl of 1.05 mM of PA solution and incubated at room temperature for 6 h before acquiring the CD spectra. 10 μl of 0.05 M EDTA was then added to the solution and further spectra were acquired immediately and again after a 6 h incubation. CD spectra were obtained from 190 nm to 300 nm at a digital integration time of 1 s, a band width of 1 nm and a data pitch of 0.1 nm.

CD (at variable temperatures)

Variable temperature CD studies were carried out with Jasco J-815 equipped with PTC-423S/15 peltier unit. Before preparing the CD samples, 1.05 mM PA solution was sonicated for 1 h. To prepare low pH samples, the PA was diluted in sodium acetate buffer or HCl solution. PA with $CaCl_2$ samples were prepared by diluting PA in a Tris buffer containing $CaCl_2$. Concentration details can be found in Table S1 (ESI†). The samples were mixed well and incubated for 24 h at room temperature for equilibration. For each measurement, 300 μl of the sample was pipetted into a 1 mm quartz cuvette which was inverted gently for mixing without damaging any assembled structures. CD spectra were obtained from 190 nm to 300 nm at a digital integration time of 4 s, a band width of 1 nm and a data pitch of 0.1 nm. Samples were heated at a rate of 0.2 °C min^{-1}, and spectra were collected at 1 °C intervals between 25 °C and 90 °C. After acquisition of the spectra, the spectra were smoothed with means movement with a convolution width of 15, which was included in the Spectra-Manager (Jasco-UK ltd) software.

FT-IR

PA solution at pH 7, PA solution mixed with $CaCl_2$ and PA solution mixed with HCl were prepared for FT-IR analysis. The PA at pH 7 sample was prepared by using 150 μl of 10 mM PA solution. The PA with $CaCl_2$ sample was prepared by mixing 125 μl of 10 mM PA solution with 25 μl of 1 M $CaCl_2$. The PA with HCl sample was prepared by mixing 125 μl of 10 mM PA solution with 25 μl of 1 M HCl. In order to obtain complete diffusion of the gelling agents, the samples were shaken overnight and then frozen and freeze-dried. 1 mg of each formulation was mixed with 100 mg of KBr and crushed thoroughly. Transmittance of the pellet was measured by a Bruker, Vertex 70 FT-IR instrument.

Zeta potential and pH measurements

Zeta potential measurements were performed with Malvern Nano-ZS zetasizer which contains a pH meter and titration system. PA at pH 7, PA at pH 2 and PA at pH 7 with $CaCl_2$ were used for zeta potential measurements. PA solutions were prepared at 0.05 wt% and the pH adjusted to 7 before use. PA was mixed with $CaCl_2$ at 1 : 5 molar ratio respectively and the pH set to 2 with 0.1 M HCl. 0.06 wt% PA solution was prepared for the pH measurement study and the pH was set to 11 before use. Titration was performed by adding 0.1 M HCl to the PA solutions. The Smoluchovski method was used to determine the zeta potential values.

Oscillatory rheology

Rheology measurements were performed with an Anton Paar Physica RM301 Rheometer operating with a 25 mm parallel plate at a 0.5 mm gap distance. Freeze-dried PA molecules were dissolved in deionized water and the pH was adjusted to 7 with 0.1 M NaOH solution. The total volume of each sample was set to 150 μl and gel formation was achieved by mixing 125 μl of PA solution (pH 7) with 25 μl of aqueous gelator solution (HCl or $CaCl_2$). The gel was prepared on the lower plate of the rheometer and gelling agents were added dropwise in order to prevent any deformation of the gel structure with a mole excess amount to ensure a higher diffusion rate and improved interaction with PA molecules. Four different concentrations of PA and gelator were investigated using time sweep oscillatory measurements. The final concentration of PA and gelators are listed in Table S2 (ESI†). The stage temperature was adjusted to 25 °C and all samples were allowed to equilibrate for 15 min before the measurements were taken to achieve stable gel formation. Wet tissue paper was placed inside the chamber around the edge of the plate to provide a humid environment and prevent solvent evaporation from the sample during the experiments. Measurements were taken for 60 min at 10 rad s^{-1} and 0.5% strain (Fig. 4).

Temperature dependent oscillatory rheology measurements were performed for PA with HCl and PA with $CaCl_2$ gels with final concentrations of; 8.5 mM PA with 833.3 mM gelator. Measurements were performed from 25 °C to 85 °C at a heating rate of 1 °C min^{-1} with a 10 rad s^{-1} frequency and 0.5% strain.

Modelling interfiber interactions

Theoretical force distance curves were calculated using the VEDA environment.[24] Tip radius was estimated to be 10 nm by comparing force–distance curves obtained on silicon and a 100 nm thick PMMA film on silicon, assuming the PMMA elastic modulus to be 3 GPa.[25] The standard DMT tip–sample interaction model[26] was used. This information together with the sample preparation technique provides sufficient information to repeat such measurements. The tip-radius is fitted, as well as the spring constant (fitted by careful calibration of the deflection signal and fitting to the Brownian Motion spectrum of the cantilever). The force–distance curve fitting was done iteratively using the VEDA tool, using silicon and PMMA as reference materials.

Results and discussion

Nanoscale morphology of the PA nanofibers was observed by SEM. The nanofiber networks formed by PA nanofibers through $CaCl_2$ or HCl addition are shown in Fig. 2a and 2b respectively. The PA nanofibers formed bundles which were favored by interfibrillar interactions mediated by hydrogen bonding, electrostatic attractions between positively and negatively charged amino acids and ion bridging formed by calcium ions. As a result of SEM imaging, no significant differences in bundle and mesh size were observed between the nanofiber network and the PA nanofibers formed through either mechanism.

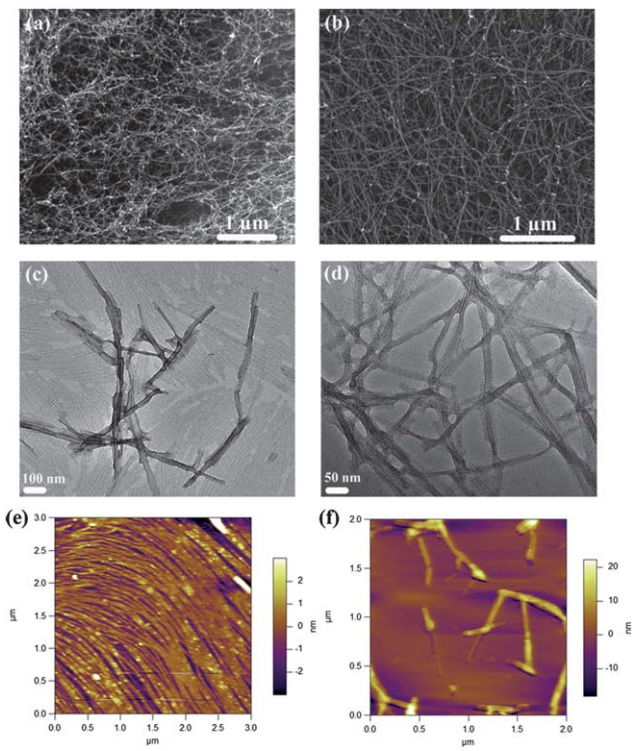

Fig. 2 Scanning electron micrographs of (a) PA with $CaCl_2$ gel, (b) PA with HCl gel (scale bars are 1 μm). Transmission electron micrographs of (c) PA with $CaCl_2$ gel and (d) PA with HCl gel. AFM topography micrographs of (e) PA with $CaCl_2$ gel and (f) PA with HCl gel.

PA nanofibers formed by addition of $CaCl_2$ or HCl solutions were visualized by transmission electron microscopy (TEM) and atomic force microscopy (AFM). TEM revealed that PA with $CaCl_2$ and PA with HCl nanofibers are around 8–10 nm in diameter and micrometres in length ((Fig. 2c, S12, 2d and S13, ESI†). The AFM results indicated that PA molecules have formed nanofibers in several lengths for both self-assembly mechanisms (Fig. 2e and 2f). However, it is noteworthy that the PA with $CaCl_2$ samples contain longer fibers whereas the PA with HCl samples contain shorter but more aggregated fibers arranged as bundles. Even though the PA with HCl and the PA with $CaCl_2$ samples are quite similar in the SEM figures, they show significant differences in the AFM images. This difference is mostly due to the formation of PA nanofiber bundles during drying of the samples for AFM imaging.

The effect of peptide secondary structure on the self-assembly process was studied by circular dichroism (CD) spectroscopy. Previous studies demonstrated that the cylindrical micelles formed by PA molecules contain β-sheets and amino acids closer to the hydrophobic tail are considered to be critical for β-sheet secondary structure.[7] The CD experiments were carried out at room temperature and at variable temperatures. PA at pH 7, PA with $CaCl_2$ and PA with HCl were studied by CD. The PA at pH 7 was analyzed to determine whether the PA molecules self-assemble into defined secondary structures without any charge screening. The PA with HCl sample was studied in order to see the effect of neutralization of charges by pH change on the secondary structure formation of the PA nanofibers. The PA with $CaCl_2$ formulation was studied to observe the effect of electrolyte addition without any pH change on secondary structure.

In the CD spectra, the spectrum for a random coil displays a signal at 195 nm whereas β-sheets display a negative band at 220 nm and a positive band at 195 nm. Fig. 3a demonstrates the CD spectra of the PA at pH 7, PA with $CaCl_2$ and PA with HCl samples. The CD studies revealed that both pH reduction and electrolyte addition self-assembly mechanisms resulted in predominantly β-sheet signals. However, the PA solution at pH 7 revealed a random coil signal. In the light of these results, the PA molecules do not self-assemble into defined secondary structures at physiological pH without charge screening ($CaCl_2$) or charge neutralization (HCl). Addition of a divalent cation (Ca^{2+}) or lowering the pH (HCl) causes charge screening and charge neutralization of these molecules. Charge screening and neutralization of PA molecules eliminate the repulsive forces and enables the formation of hydrogen bonding networks. Formation of hydrogen bonding networks together with hydrophobic collapse of alkyl groups leads to the formation of self-assembled nanostructures.[27] Charge screening (by Ca^{2+}) and charge neutralization (by H^+) of the PA molecules have been studied by measuring the zeta potential of the three formulations (Fig. S3a, ESI†). The PA molecules at pH 7 were neutralized by the addition of $CaCl_2$ (1 : 5 molar ratio) or adjusting the pH to 2. The pH dependent charge neutralization of PA molecules is shown in

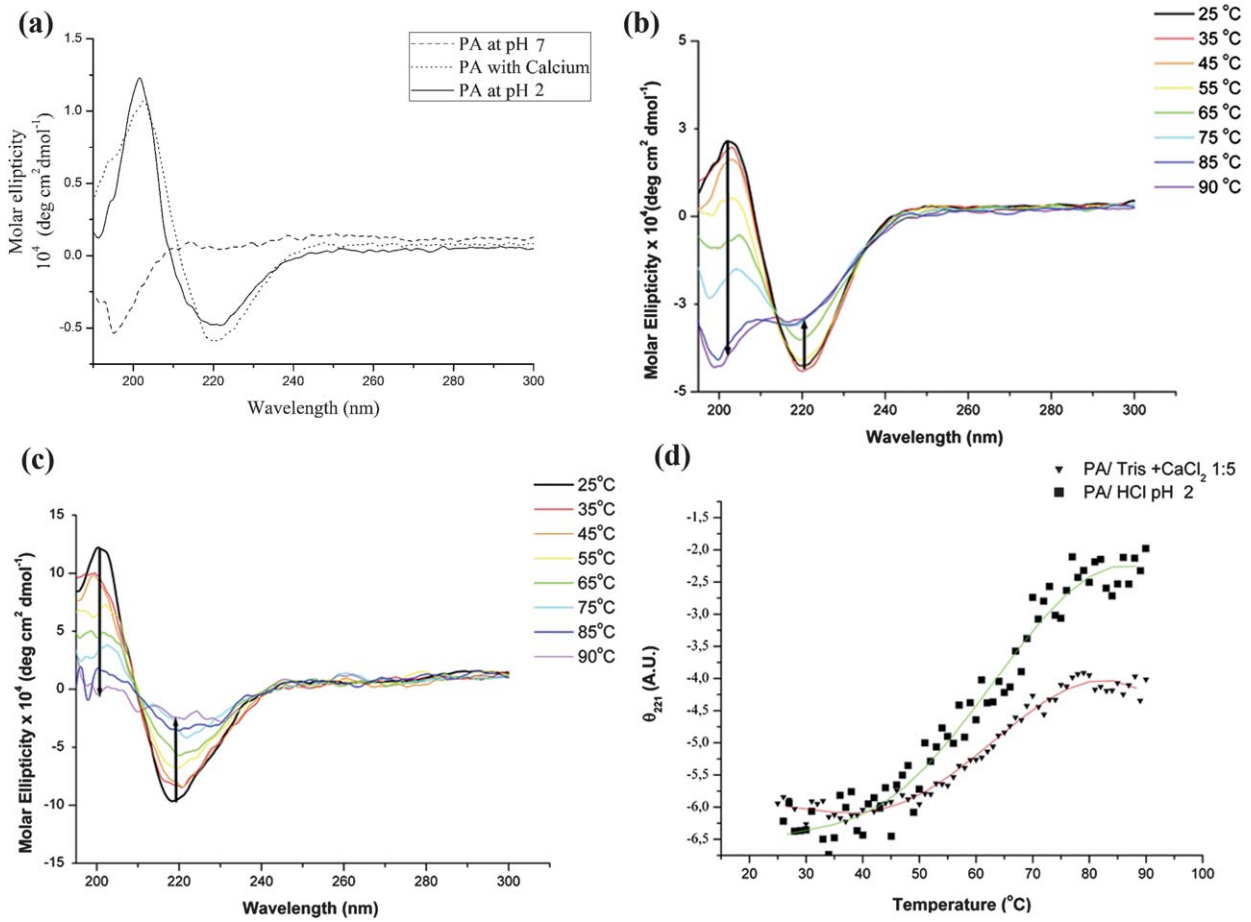

Fig. 3 (a) Circular dichroism spectra of the PA at pH 7, PA with HCl and PA with $CaCl_2$ at room temperature. Temperature dependent circular dichroism spectra of (b) the PA with $CaCl_2$, (c) PA with HCl (pH 2). (d) Ellipticity at 221 nm for PA with $CaCl_2$ and PA with HCl (pH 2) monitored between 25 °C and 90 °C.

Fig. S3b†. The CD and zeta potential data suggest that neutralization of the PA molecules leads to aggregation of these molecules and the formation of a β-sheet secondary structure. Thus, neutralization of charges enables the PA molecules to self-assemble into defined nanostructures. Addition of EDTA to the PA with $CaCl_2$ sample destroyed the β-sheet assembly and resulted in random coil signals in the CD spectrum due to the removal of Ca^{2+} ions from the solution (Fig. S4, ESI†). Charge screening (by Ca^{2+}) and charge neutralization (H^+) is mainly brought about by dynamic interactions which can be reversed by the isolation of neutralizers from the environment.

FT-IR spectroscopy was also used for analysis of the three formulations (pH 7, pH 2 and pH 7 with Ca^{2+}) used in the CD experiments. The FT-IR spectra for all three formulations exhibit an amide I peak at 1633 cm^{-1} which is typical for β-sheets[28] (Fig. S5, ESI†). Although a β-sheet signal is expected from samples of pH 2 and pH 7 with calcium ions, the pH 7 sample also exhibited β-sheet singals. It is likely that the β-sheet signal observed in the pH 7 sample is due to stacking and close packing of the PA molecules during the freeze-drying process. These results suggest that both FT-IR and CD studies are consistent, indicating the effect of pH screening and addition of divalent cations on the secondary structure of the PA molecules.

Variable temperature CD studies enabled the monitoring of the thermal denaturation of the β-sheet secondary structure triggered by $CaCl_2$ addition or the lowering of the pH. At 25 °C, characteristic β-sheet traces with negative bands at about 220 nm and positive bands around 202 nm were observed for the $CaCl_2$ and pH 2 samples. The β-sheet signals gradually diminished while heating from 25 °C to 90 °C indicating denaturation of the peptide assemblies formed by β-sheet structures (Fig. 3b, 3c). Both $CaCl_2$ and HCl (pH 2) samples exhibited similar melting profiles with melting temperatures around 60–65 °C (Fig. 3d). At pH 3.6 and in the presence of 1.43 molar equivalents of $CaCl_2$, the CD spectra at room temperature possess red shifted bands and strong signals at the π–π* transition region (Fig. S6a, S6b†) which may additionally indicate β-sheets existing in a twisted conformation rather than planar in these samples.[29] At pH 3.6, the charges on the PA molecules are partially neutralized (Fig. S7, ESI†). At this particular pH and $CaCl_2$ concentration, full charge screening does not occur. Therefore, electrostatic interactions may be causing the PAs to become assembled in twisted β-sheet conformation.

The mechanical properties of the gels formed by PA nanofibers were studied by oscillatory rheology. The storage modulus (G') and loss modulus (G'') were recorded as a function of time and

temperature. The results of time sweep rheology experiments of the PA with $CaCl_2$ and PA with HCl gels at different concentrations are shown in Fig. 4. The storage moduli of the gels increased rapidly and leveled off at a plateau for each concentration because of the aging process (Fig. S8–S11, ESI†). For all concentrations, the G' value higher than G'' implies that these gels act as elastic solids.[30] It is noteworthy that the viscoelastic behavior of the gels formed by HCl or $CaCl_2$ addition demonstrate significant differences. Time dependent storage and loss moduli values of the gels were compared. The gels formed by the same PA molecules at identical concentrations with different gelators have considerable differences in stiffness due to changes in the self-assembly mechanism (Fig. 4). Fig. 5 shows the effect of concentration on the storage moduli of the gels.

Temperature dependent oscillatory rheology was performed in order to investigate the behavior of PA gels with respect to temperature change for different gelation mechanisms (Fig. 6). These PA gels respond significantly differently to an increase in temperature. The PA with HCl gels started to lose their mechanical integrity at 30–40 °C whereas the PA with $CaCl_2$ gels started to denature at around 60–70 °C. The stability of the PA with $CaCl_2$ gels might be due to calcium bridging resulting in interfiber interactions and covering the PA fibers with calcium ions. It is widely known that metalloproteins have increased stability against temperature and this effect is observed in hot spring bacteria, proteins of which are not denatured at high temperatures.[31,32] However, the PA with HCl gels cannot withstand high temperature. There are some differences in the start and end points of both storage and loss moduli between time and temperature dependent measurements because of the changes in experimental set up and time interval of data points.

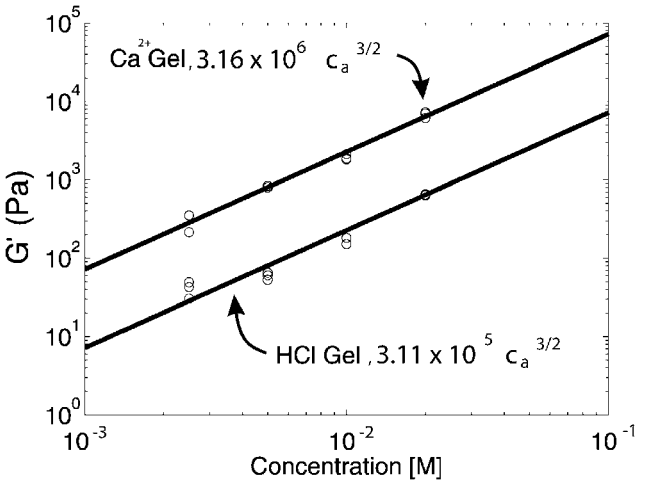

Fig. 5 Macroscopic rheological study of the gels prepared with $CaCl_2$ and HCl shows that both gels scale with a 3/2 exponent on concentration, calcium gels being typically an order of magnitude stronger at the same concentration.

In the CD spectra, the denaturation profiles due to temperature increase were similar for cation triggered and pH triggered PA assemblies. However, different thermo-mechanical responses were observed for PAs gelled with $CaCl_2$ or HCl by temperature dependent oscillatory rheology study. It should be noted that the

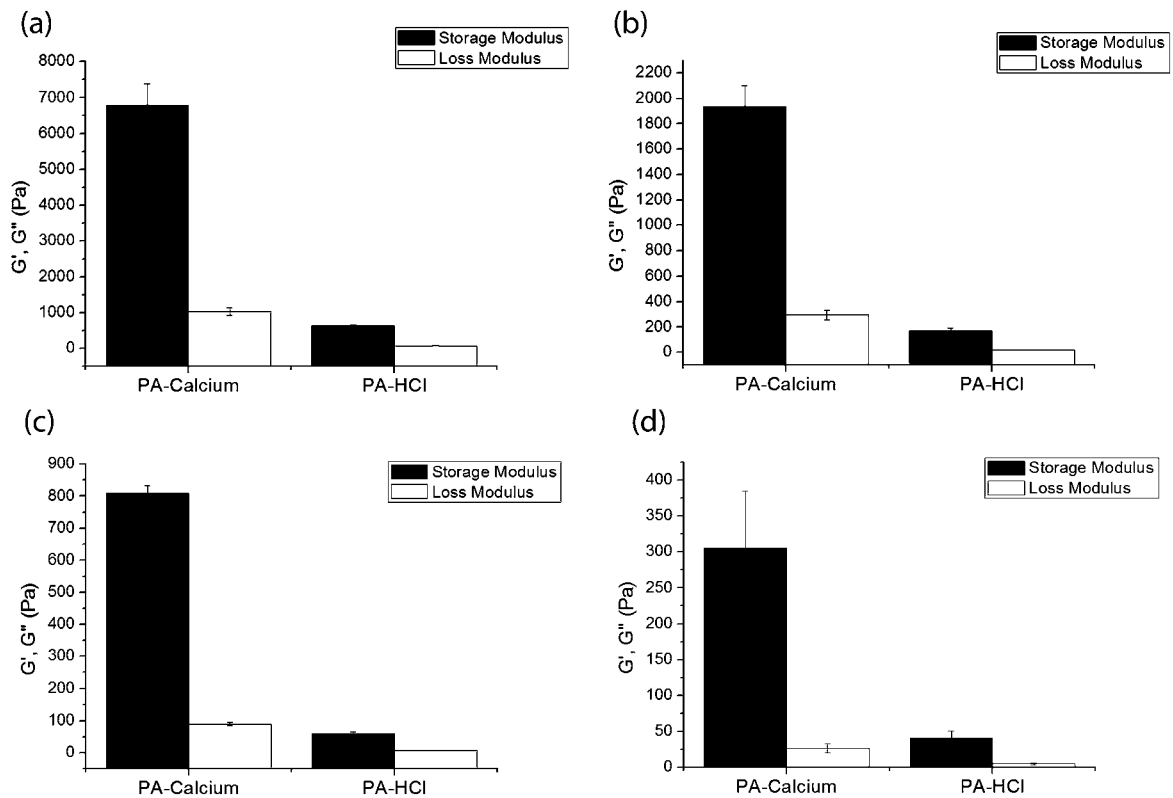

Fig. 4 Time sweep oscillatory rheology measurements (t: 60 min) of PA with $CaCl_2$ and PA with HCl gels (a) 16.9 mM PA and 1.6 M HCl or $CaCl_2$, (b) 8.5 mM PA and 0.833 M HCl or $CaCl_2$, (c) 4.2 mM PA and 416.7 mM HCl or $CaCl_2$ and (d) 2.1 mM PA and 208.3 mM HCl or $CaCl_2$.

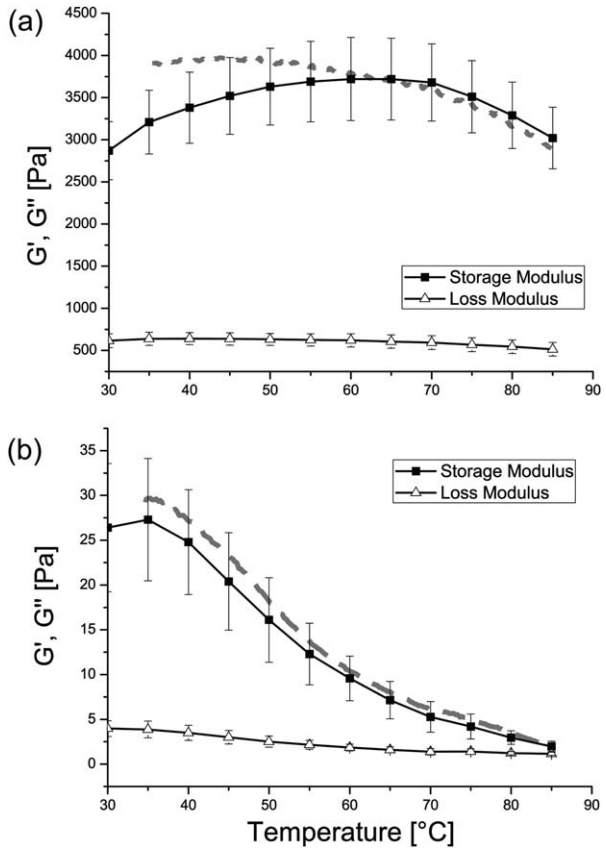

Fig. 6 Temperature dependent oscillatory rheology of (a) PA with $CaCl_2$ gels (b) PA with HCl gels. Dashed lines show the data corrected for aging and time dependent stiffening of the gels.

gels used had concentrations at mM scale in the rheology studies whereas at the scale of 10–150 μM in the CD measurements. Thus, melting curves obtained with CD are more likely to be a reflection of breaking of hydrogen bonds within assemblies, as a result of the nature of the intrafibrillar attractions. On the other hand, the responses observed with oscillatory rheology are related to the three-dimensional network mechanics in which interfibrillar attractions are more prominent than intrafibrillar bondings.

Previously, entropic and energetic descriptions of the viscoelastic properties of gels were studied in order to explain the dependence of gel stiffness on different factors such as concentration or temperature. There are a number of different approaches describing the mechanical properties of gels[33] and depending on the micro and nanostructure of the gels, different models are appropriate for explaining the observed viscoelastic properties. Assuming entropic forces dominate the mechanics of polymeric gels, MacKintosh scaling[20] has been used to predict the dependence of stiffness on concentration. In the original work by MacKintosh *et al.*, the stiffness of the gel is expressed in terms of the bending modulus of the fiber κ, the mesh size ξ and the entanglement length L_e, as $G' \sim \frac{\kappa^2}{k_B T}\xi^{-2}L_e^{-3}$ where k_B is the Boltzmann constant, and T is the temperature. Several underlying assumptions in the derivation of the MacKintosh scaling lead to the stiffness of the form

$$G' \sim \kappa\left(\frac{\kappa}{k_B T}\right)^{\frac{2}{5}}(ac_A)^{\frac{11}{5}} \quad (1)$$

where c_A is the concentration and a is the monomer size. In a case where the fiber bending modulus is not dependent on the concentration, stiffness of the gel is roughly proportional to the square of concentration, $G' \propto c_A^{\frac{11}{5}}$. Also, the softening of such gels is predicted for increasing temperatures, with a weak ($T^{-2/5}$) temperature dependence. For self-assembled systems, the MacKintosh model has been insufficient to explain the observed scaling of gel stiffness as a function of concentration.[30] In contrast, the stiffness of the gels can be described using elastic deformation models, assuming individual fibers are rigid rods with frozen or free hinges at the cross-links.[34] In the case of the freely hinged rigid rod network model, the stiffness is expected to scale with concentration as $G' \propto c_A^{\frac{3}{2}}$. The cellular solid model[35] describes a similar energetic (elastic) approach with non-free hinges and estimate a scaling of $G' \propto c_A^2$, or $G' \approx 3E_S(c_A/\rho_s)^2/8$, where E_S is the Young's modulus of the bundles and ρ_s is the density within the bundles.

In self-assembled PA nanofiber networks, an elastic rod network is present in the gels based on SEM micrographs (Fig. 2). Therefore, we assumed that a rigid rod model may be applicable to describe the mechanical properties. Based on the elastic rod network model given in the literature,[34] rod network with frozen crosslinks is expected to have a scaling given by $G' \propto c_A^2$ whereas the freely hinged rod network has a slightly different scaling, namely $G' \propto c_A^{3/2}$. In the PA gels, the stiffness of the gels was observed to scale with $G' \propto c_A^{3/2}$ and it was also observed that the calcium gels were about an order of magnitude stronger than HCl gels (Fig. 5). The fiber bundles were observed to be fixed at the cross-over points, freely hinged network model agrees well with our observations, as well as some of the previous observations by other groups.[30]

In order to understand the underlying mechanisms in determination of the gel stiffness, the dependence of stiffness on parameters other than concentration of the gels (such as nanoscale structure or chemical properties leading to different bond strengths within or among fibers) must be considered. Based on the SEM micrographs and scaling of the elasticity with concentration, we assume that a rod network model is valid in

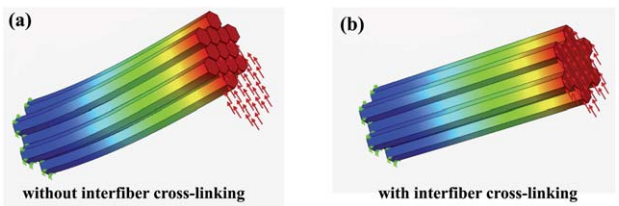

Fig. 7 Static mechanical finite element modeling of bending of fiber bundles is shown. A directional force load applied at one end, while keeping the other end fixed. Here, the same force is applied to individual fibers and deflections are drawn with same scale. (a) A maximum deflection of 289.2 distance units is observed for free fibers as compared to (b) a deflection of 17.1 distance units for the cross-linked fibers. Cross-linking of the fibers within the bundle increases the overall bending stiffness of the bundle (about 17 times for this example involving 13 fibers per bundle).

describing the supramolecular gels. In the rod network model, the gel stiffness depends on many factors including the bending spring constant of individual fibers. In the case of rigid rod model, the bending spring constant k_s of a rod of diameter t and length L, made of a material with Young's (elastic) modulus E is given by

$$k_s \sim \frac{Et^4}{4L^3} \quad ([2])$$

Here, the bending modulus is related to elasticity and geometry as $\kappa \sim Et^4$. The strength of individual fibers determines the overall stiffness of the gel if no bundling is present. If bundling is present, the bending spring constant of the bundle is observed to be strongly dependent on the interfiber bonding. It can be recognized that, if fibers form bundles with strong interfiber bonds (cross-linking of fibers), all fibers in the bundle behave as a continuous elastic material and the bending modulus of the bundle scales with the fourth power of the bundle diameter, $\kappa \propto t^4$. If such a strong cross-linking is not present, the fibers behave as individual elements and the scaling of the bundle bending modulus merely goes as proportional to the square of the bundle diameter (asymptotically), $\kappa \propto t^2$. This behavior can be verified by finite element modeling (Fig. 7). If the bundles are subjected to a bending moment, depending on the strength of the interfiber bonds, delamination may occur between fibers and subgroups of fibers may emerge, resulting in a mixture of bonded and unbonded sub-bundles. In such a case, the bending modulus κ of the bundles are dependent on the bundle diameter t as $\kappa \propto t^x$, where $2 < x < 4$. It must be noted that the scaling of the elasticity with bundle diameter is not directly related to the scaling on concentration. The discussion is aimed to explain the observed 10 fold increase in gel elastic modulus for calcium gels as compared to HCl gels. In the AFM micrographs (Fig. 2e and 2f), it was observed that nanofibers formed in the presence of Ca^{2+} tend to form long fibers. The calcium fibers were also seen to organize into parallel fibers on the surface, forming ordered monolayer films. In contrast, the pH induced nanostructures are short fibers that do not form into such monolayer films. These observations may suggest that calcium gels have stronger interfiber and intrafiber bonds.

When individual fibers are considered, interfiber bonds do not play a role in the elasticity, only intrafiber bonds do. Also, interfiber bonding has less effect on apparent elasticity in an indentation measurement performed on a thin film of nanofibers. In such a measurement, when an AFM tip interacts with fibers, forces within a bundle of fibers are normal to the fiber sidewalls and slippage due to weak interfiber bonds is not significant (Fig. 8a). Therefore, intrafiber and interfiber contributions to the stiffness may be distinguished by comparing the stiffness of individual fibers or bundles measured using AFM indentation with macroscopic rheological measurements.

In AFM indentation measurements, it was observed that thin films of fibers composed of both Ca^{2+} and HCl gels displayed an apparent elastic modulus of ~200 and ~100 MPa respectively (Fig. 8b). SEM micrographs of gels show that both the calcium gels and HCl gels have similar bundle radii, mesh size and entanglement lengths for a given concentration. Based on the AFM indentation measurements, the Gibson formula, $G' \approx 3E_s(c_A/\rho_s)^2/8$ predicts that calcium gels should have about 2 times the elastic modulus of the HCl gels. However, it was observed in

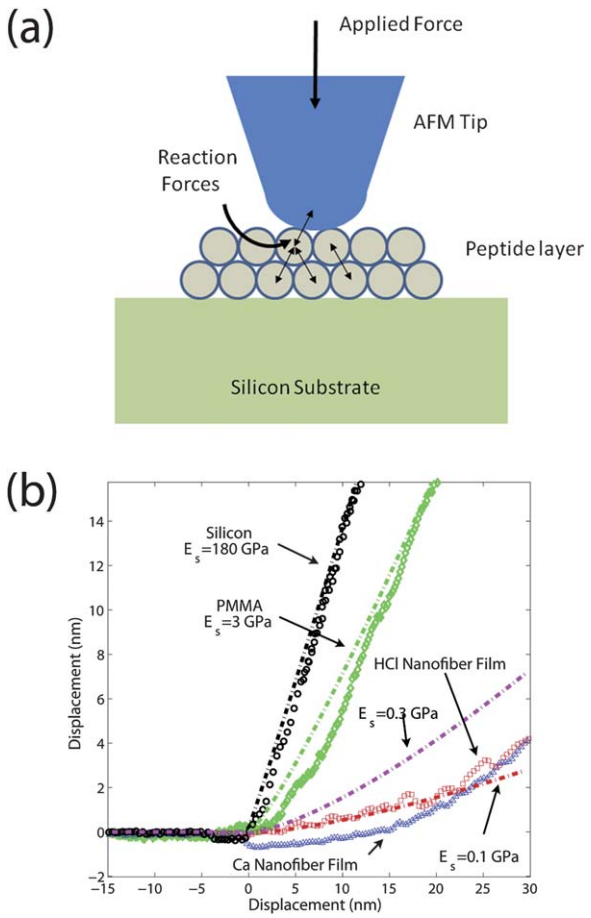

Fig. 8 (a) In an indentation measurement on films of nanofibers, interfiber forces are mostly normal to the fiber surface and interfiber crosslinking has less effect on apparent material stiffness. (b) Indentation measurements on silicon ($E = 180$ GPa) (black circles) and PMMA thin films ($E = 3$ GPa) (green squares) were performed for calibration and are shown along with theoretical fits. Using the same tip and AFM configuration, measurements performed on thin films of PA with HCl (red diamonds) and PA with calcium fibers (blue triangles) suggest that films of fibers prepared by both PA with calcium and HCl nanofibers have elastic moduli of about 0.1 GPa, PA with calcium fiber films having slightly greater elastic modulus (~200 MPa). Approach curves are used for data fitting.

the rheology measurements that calcium gels are about an order of magnitude stiffer than HCl gels. Based on continuum mechanics and finite element analysis, the apparent discrepancy may be attributed to the presence of stronger interfiber cross-linking in calcium gels.

It must also be noted that, the temperature dependence of the gel elasticity for different scaling models (*e.g.* MacKintosh and elastic rod network) may be significantly different. For the MacKintosh model, the softening of such gels is predicted for increasing temperatures, with a weak explicit temperature dependence, $T^{-2/5}$. However, if the elastic rod network model (with bundles of fibers) is considered, the temperature dependence is implicit in the changes of the effective Young's modulus of the individual fibers and the temperature dependence of interfiber crosslinking strength. A decrease of gel stiffness with increasing temperature is observed in our gels (Fig. 6). The

observed behavior may be explained through the presence of characteristic temperatures beyond which interfiber or intrafiber bonds start to break. A phenomenological expression for the temperature dependent elasticity of an individual fiber can be given as[36]

$$G' \propto \frac{G'_0}{1 + \alpha \exp\left(\frac{T - T_0}{D_0}\right)} \quad ([3])$$

where G_0 is the low temperature elastic modulus, α, D_0 and T_0 are material dependent constants. In this case, the temperature dependence of the overall elastic modulus may be the result of the reduction in elastic moduli of individual fibers (intrafiber bonds) and/or reduced bundle stiffness due to the breaking of interfiber bonds. For PA with HCl gels, T_0 is lower than 35 °C while for the PA with calcium gels T_0 is higher than 60 °C. Considering the CD data shown in Fig. 3d, a temperature of $T_0 \sim 60$ °C corresponds to the disintegration of the sheets inside the fibers. Therefore, for both HCl and calcium gels, we would expect to have the individual fiber elasticity to be similar, below 60 °C. However, gel elasticity depends on the elasticity of the bundles and may be different for HCl and calcium gels, even if individual fibers have similar mechanical properties. Indeed, the difference shown in Fig. 6a and 6b indicates that HCl gels lose their elastic modulus at much lower temperatures ($T_0 < 35$ °C) compared to the calcium gels ($T_0 \sim 60$ °C). Presence of multiple mechanisms (namely, the effect of interfiber bonds and intrafiber bonds) that determine the gel elasticity suggests a description of the elasticity with the form

$$G' \propto \frac{\left(G'_0 + G'_1\right) - (G'_0 - G'_1)\tanh\left(\frac{T - T_1}{D_1}\right)}{2\left[1 + \alpha \exp\left(\frac{T - T_0}{D_0}\right)\right]} \quad ([4])$$

where G'_0 and G'_1 are low temperature elastic moduli with and without interfiber cross-linking, T_1 is a transition temperature from cross-linked to free fibers and D_1 is a parameter that defines the temperature range over which interfiber bonds are eliminated. Although in our experiments we do not determine the values for G'_0 and G'_1, T_1 and D_1, the phenomenological description in eqn (4) is given for better intuition.

Conclusion

In conclusion, we studied the elasticity of self-assembled supramolecular peptide amphiphile nanofiber gels. Macroscopic (rheological) and nanoscale (AFM) measurements yielded significantly differing elastic moduli for gels prepared using calcium or HCl as the gelation agent. Circular dichroism measurements suggest that intrafiber bonds begin to disintegrate above 60 °C for both calcium and HCl gels. However, gel elasticity displays different temperature dependence for the two different gels. These observations suggest that the model describing gel stiffness must contain effects other than those affecting single fiber elasticity. Based on an energetic model of elastic rod networks, along with continuum mechanical models of bundles of rods, we point out that the discrepancy in gel stiffness for the calcium and HCl gels may arise from the difference in strength of interfiber bonds.

Acknowledgements

This work is supported in part by the Marie Curie IRG grant 231019 and TUBITAK 110M355 and 107T547. Authors thank to M. Guler for help in TEM, R. Mammadov for help in AFM and Z. Erdogan for help in LC-MS.

References

1 H. Cui, M. J. Webber and S. I. Stupp, *Biopolymers*, 2010, **94**, 1–18.
2 J. C. Stendahl, M. S. Rao, M. O. Guler and S. I. Stupp, *Adv. Funct. Mater.*, 2006, **16**, 499–508.
3 J. D. Hartgerink, E. Beniash and S. I. Stupp, *Proc. Natl. Acad. Sci. U. S. A.*, 2002, **99**, 5133–5138.
4 H. A. Behanna, J. J. Donners, A. C. Gordon and S. I. Stupp, *J. Am. Chem. Soc.*, 2005, **127**, 1193–1200.
5 Y. S. Velichko, S. I. Stupp and M. O. de la Cruz, *J. Phys. Chem. B*, 2008, **112**, 2326–2334.
6 S. Ganesh, S. Prakash and R. Jayakumar, *Biopolymers*, 2003, **70**, 346–354.
7 S. E. Paramonov, H. W. Jun and J. D. Hartgerink, *J. Am. Chem. Soc.*, 2006, **128**, 7291–7298.
8 E. Beniash, J. D. Hartgerink, H. Storrie, J. C. Stendahl and S. I. Stupp, *Acta Biomater.*, 2005, **1**, 387–397.
9 S. Zhang, T. Holmes, C. Lockshin and A. Rich, *Proc. Natl. Acad. Sci. U. S. A.*, 1993, **90**, 3334–3338.
10 M. O. Guler, L. Hsu, S. Soukasene, D. A. Harrington, J. F. Hulvat and S. I. Stupp, *Biomacromolecules*, 2006, **7**, 1855–1863.
11 S. R. Bull, M. O. Guler, R. E. Bras, P. N. Venkatasubramanian, S. I. Stupp and T. J. Meade, *Bioconjugate Chem.*, 2005, **16**, 1343–1348.
12 K. L. Niece, J. D. Hartgerink, J. J. Donners and S. I. Stupp, *J. Am. Chem. Soc.*, 2003, **125**, 7146–7147.
13 G. A. Silva, C. Czeisler, K. L. Niece, E. Beniash, D. A. Harrington, J. A. Kessler and S. I. Stupp, *Science*, 2004, **303**, 1352–1355.
14 J. D. Hartgerink, E. Beniash and S. I. Stupp, *Science*, 2001, **294**, 1684–1688.
15 T. D. Sargeant, M. O. Guler, S. M. Oppenheimer, A. Mata, R. L. Satcher, D. C. Dunand and S. I. Stupp, *Biomaterials*, 2008, **29**, 161–171.
16 V. M. Tysseling-Mattiace, V. Sahni, K. L. Niece, D. Birch, C. Czeisler, M. G. Fehlings, S. I. Stupp and J. A. Kessler, *J. Neurosci.*, 2008, **28**, 3814–3823.
17 A. J. Engler, S. Sen, H. L. Sweeney and D. E. Discher, *Cell*, 2006, **126**, 677–689.
18 D. E. Ingber, *J. Cell Sci.*, 2003, **116**, 1397–1408.
19 D. E. Ingber, *J. Cell Sci.*, 2003, **116**, 1157–1173.
20 F. C. MacKintosh, J. Kas and P. A. Janmey, *Phys. Rev. Lett.*, 1995, **75**, 4425–4428.
21 R. Tharmann, M. M. Claessens and A. R. Bausch, *Biophys. J.*, 2006, **90**, 2622–2627.
22 M. D. Pierschbacher and E. Ruoslahti, *Nature*, 1984, **309**, 30–33.
23 A. Rosa-Zeiser, *et al.*, *Meas. Sci. Technol.*, 1997, **8**, 1333.
24 J. Melcher, S. Hu and A. Raman, *Rev. Sci. Instrum.*, 2008, **79**, 061301.
25 O. Sahin, S. Magonov, C. Su, C. F. Quate and O. Solgaard, *Nat. Nanotechnol.*, 2007, **2**, 507–514.
26 B. V. Derjaguin, V. M. Muller and Y. P. Toporov, *Prog. Surf. Sci.*, 1994, **45**, 131–143.
27 S. Tsonchev, K. L. Niece, G. C. Schatz, M. A. Ratner and S. I. Stupp, *J. Phys. Chem. B*, 2008, **112**, 441–447.
28 S. Krimm and J. Bandekar, *Adv. Protein Chem.*, 1986, **38**, 181–364.
29 M. C. Manning, M. Illangasekare and R. W. Woody, *Biophys. Chem.*, 1988, **31**, 77–86.
30 M. A. Greenfield, J. R. Hoffman, M. O. de la Cruz and S. I. Stupp, *Langmuir*, 2010, **26**, 3641–3647.
31 V. Bernal and P. Jelen, *J. Dairy Sci.*, 1984, **67**, 2452–2454.
32 A. Spungin and S. Blumberg, *Eur. J. Biochem.*, 1989, **183**, 471–477.
33 M. O. Piepenbrock, G. O. Lloyd, N. Clarke and J. W. Steed, *Chem. Rev.*, 2010, **110**, 1960–2004.
34 J. L. Jones and C. M. Marques, *J. Phys.*, 1990, **51**, 1113–1127.
35 L. J. Gibson and M. F. Ashby, *Cellular Solids: Structure and Properties*, Cambridge University Press, Cambridge, New York, 1997.
36 D. C. Lin, J. F. Douglas and F. Horkay, *Soft Matter*, 2010, **6**, 3548–3561.

